Additive Manufacturing of Cupric Oxide via Direct Ink Writing

Fabricación aditiva de óxido cúprico mediante escritura directa con tinta

Fabricação aditiva de óxido cúprico por escrita direta de tinta

Muhammad Ali [1], Shaheryar A. Khan [2] (*), Aqueel Shah [3], Antash Najib [4], Abbas Hussain [5]

Recibido: 18/08/2025 Aceptado: 24/11/2025

Summary. - The DIW approach offers numerous benefits, including expedited prototyping, cost-effectiveness, reduced waste in manufacturing, and enhanced design flexibility. It's currently a popular production method for building materials and has great potential for porous and electronic materials. In this study, porous cupric oxide (CuO) ceramics were fabricated using a direct ink writing (DIW) approach based on a copper particle–laden aqueous precursor. The ink formulation was optimized to achieve stable extrusion and crack-free green bodies, yielding a final composition of 68.0 wt% Cu, 31.3 wt% water, and 0.6 wt% CMC. Following oxidation and sintering in air, the printed structures exhibited a bulk density of 3.60 ± 0.20 g cm^{-3} and a corresponding theoretical porosity of 43.7 ± 0.9%. X-ray diffraction confirmed nearly phase-pure monoclinic CuO with no detectable Cu or Cu_2O residues. The printed components exhibited an interconnected, porous microstructure and a four-point-probe resistivity of 10.5 ± 0.3 Ω·m at 25 °C, reflecting the influence of high porosity on charge transport. The DIW route demonstrated here provides a controllable pathway for producing porous CuO architectures with tunable microstructure and moderate electrical conductivity. These characteristics suggest potential applicability in gas filtration, catalytic supports, and electrochemical sensing; however, device-level validation is still required to fully assess functional performance.

Keywords: Advanced Ceramics, Direct Ink Writing, Additive Manufacturing, Copper Oxide, Cupric Oxide, Binder, Ceramics, Green Body, Brown Body, Sintered Ceramic, Resistivity Analysis of Ceramic, Aqueous Binder Slurry, Particle Laden Slurry

(*) Corresponding author.

[1] Postgraduate Student, National University of Sciences and Technology (Pakistan), ime.322.ali@gmail.com,
ORCID iD: https://orcid.org/0009-0006-8014-5737

[2] Associate Professor and Head of the Department of Mechanical Engineering., DHA Suffa University (Pakistan), shaheryar.atta@dsu.edu.pk,
ORCID iD: https://orcid.org/0000-0003-1600-7322

[3] Professor, National University of Sciences and Technology (Pakistan), a.shah@smme.nust.edu.pk,
ORCID iD: https://orcid.org/0000-0002-4845-9350

[4] Assistant Professor, National University of Sciences and Technology (Pakistan), antash.najib@pnec.nust.edu.pk,
ORCID iD: https://orcid.org/0000-0002-4845-9350

[5] Assistant Professor, National University of Sciences and Technology (Pakistan), abbas.hussain@pnec.nust.edu.pk,
ORCID iD: https://orcid.org/0009-0008-1680-6507

Memoria Investigaciones en Ingeniería, núm. 30 (2026). pp. 14-29
https://doi.org/10.36561/ING.30.3
ISSN 2301-1092 • ISSN (en línea) 2301-1106 – Universidad de Montevideo, Uruguay

Resumen. - *El método DIW ofrece numerosas ventajas, como la creación rápida de prototipos, la rentabilidad, la reducción de residuos en la fabricación y una mayor flexibilidad de diseño. Actualmente es un método de producción popular para materiales de construcción y tiene un gran potencial para materiales porosos y electrónicos. En este estudio, se fabricaron cerámicas porosas de óxido cúprico (CuO) utilizando un método de escritura directa con tinta (DIW) basado en un precursor acuoso cargado con partículas de cobre. La formulación de la tinta se optimizó para lograr una extrusión estable y cuerpos verdes sin grietas, obteniendo una composición final de 68,0 % en peso de Cu, 31,3 % en peso de agua y 0,6 % en peso de CMC. Tras la oxidación y sinterización al aire, las estructuras impresas mostraron una densidad aparente de 3,60 ± 0,20 g cm⁻³ y una porosidad teórica correspondiente de 43,7 ± 0,9 %. La difracción de rayos X confirmó CuO monoclínico casi puro en fase, sin residuos detectables de Cu o Cu_2O. Los componentes impresos exhibieron una microestructura porosa interconectada y una resistividad de cuatro puntas de 10,5 ± 0,3 Ω·m a 25 °C, lo que refleja la influencia de la alta porosidad en el transporte de carga. La ruta de impresión directa con tinta (DIW) demostrada aquí proporciona una vía controlable para producir arquitecturas porosas de CuO con microestructura ajustable y conductividad eléctrica moderada. Estas características sugieren una posible aplicabilidad en filtración de gases, soportes catalíticos y detección electroquímica; sin embargo, aún se requiere una validación a nivel de dispositivo para evaluar completamente su rendimiento funcional.*

Palabras clave: *Cerámica avanzada, Impresión directa con tinta, Fabricación aditiva, Óxido de cobre, Óxido cúprico, Aglutinante, Cerámica, Cuerpo verde, Cuerpo marrón, Cerámica sinterizada, Análisis de resistividad de cerámica, Suspensión acuosa de aglutinante, Suspensión con partículas*

Resumo. ***-*** *A abordagem de escrita direta de tinta (DIW) oferece inúmeros benefícios, incluindo prototipagem acelerada, custo-benefício, redução de desperdício na fabricação e maior flexibilidade de design. Atualmente, é um método de produção popular para materiais de construção e tem grande potencial para materiais porosos e eletrônicos. Neste estudo, cerâmicas porosas de óxido cúprico (CuO) foram fabricadas utilizando uma abordagem de escrita direta de tinta (DIW) baseada em um precursor aquoso carregado com partículas de cobre. A formulação da tinta foi otimizada para obter extrusão estável e corpos verdes sem trincas, resultando em uma composição final de 68,0% em peso de Cu, 31,3% em peso de água e 0,6% em peso de CMC. Após oxidação e sinterização ao ar, as estruturas impressas apresentaram uma densidade aparente de 3,60 ± 0,20 g cm⁻³ e uma porosidade teórica correspondente de 43,7 ± 0,9%. A difração de raios X confirmou a presença de CuO monoclínico quase puro, sem resíduos detectáveis de Cu ou Cu_2O. Os componentes impressos exibiram uma microestrutura porosa interconectada e uma resistividade de quatro pontos de 10,5 ± 0,3 Ω·m a 25 °C, refletindo a influência da alta porosidade no transporte de carga. A rota DIW demonstrada aqui fornece um caminho controlável para produzir arquiteturas porosas de CuO com microestrutura ajustável e condutividade elétrica moderada. Essas características sugerem potencial aplicabilidade em filtração de gases, suportes catalíticos e sensores eletroquímicos; no entanto, a validação em nível de dispositivo ainda é necessária para avaliar completamente o desempenho funcional.*

Palavras-chave: *Cerâmicas Avançadas, Impressão Direta de Tinta, Manufatura Aditiva, Óxido de Cobre, Óxido Cúprico, Aglutinante, Cerâmicas, Corpo Verde, Corpo Marrom, Cerâmica Sinterizada, Análise de Resistividade de Cerâmica, Suspensão Aquosa de Aglutinante, Suspensão com Partículas*

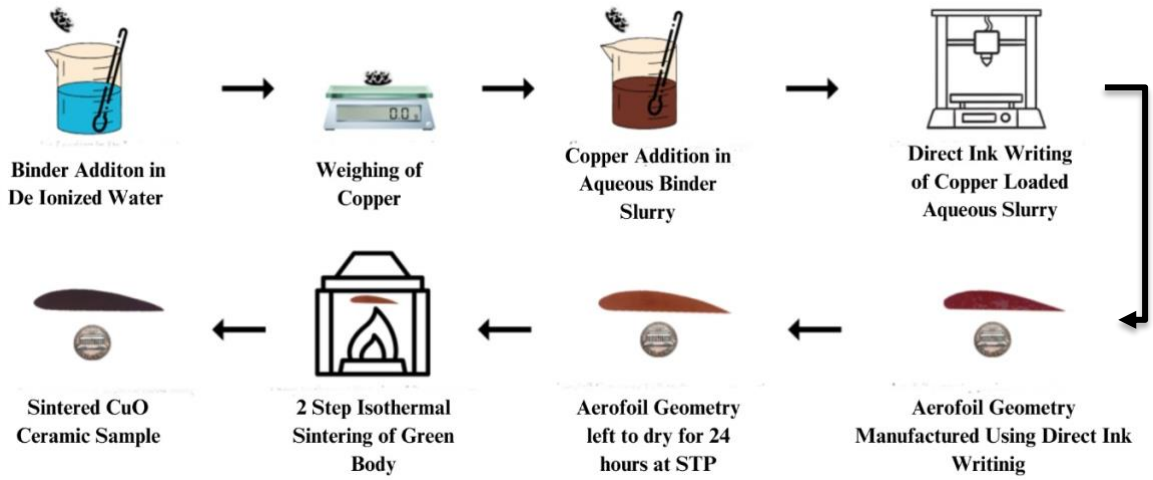

Graphical abstract.

1. Introduction. - The demand for materials with enhanced performance has created an everlasting need for the emergence of advanced materials. In today's world, advanced ceramics have primarily supplanted traditional materials. This technological change is motivated and boosted by the Asian markets in Japan and China [1].

Ceramics are well-known materials among other inorganic materials for their peculiar characteristics due to their chemical and physical properties [2]. High hardness, high strength, low thermal conductivity, and biocompatibility are some of the unique characteristics of advanced ceramics [3–6]. These materials have an enhanced resistance to wear governed by their microstructures that enable their application in various areas such as aerospace, biomedical, solar cells, fuel cells, heat exchangers, turbines, and piezo-electric devices [7].

Cupric oxide (CuO) is a black-colored ceramic material known as cupric oxide or copper (ii) oxide [8]. It is a transition metal oxide with a high surface-to-volume ratio, porosity, and monoclinic crystal structure [9,10]. It holds unique importance due to its comparable efficiency as a catalytic agent, superconducting property, anti-microbial agent, and energy-storing characteristics [9,11,12]. It is used in various domains today, including electronics, biomedical devices, energy harvesting systems, chemical catalysts for different chemical reactions, solid self-lubricants, and anti-microbial textiles [13–15]. It is used as a p-type semiconductor and magnetic storage media, finding its application in capacitors, electrodes, and different gas-sensing probes [16–19]. It is used to sense gases in the atmosphere and different biomedical sensing devices, including but not limited to CO_2, NO_2, H_2, H_2S, CO, benzyne, alcohol, ethanol, and methanol [10,20–24]. Studies show that CuO has the potential to replace the graphite anodes in lithium-ion batteries, as it is less expensive, safer, and more environmentally favorable than graphite [25]. CuO-based biomedical instruments detect blood protein patterns and blood glucose levels [16]. CuO also serves the environment by removing pollutants from the aqueous environment, including fluorides, arsenic, benzene, and toluene [26–28]. Its adsorption property removes lead, acrylic acid, and ciprofloxacin from different media, making CuO a good choice as a water-treating agent [26].

Conventional techniques for producing monolithic ceramic parts have many disadvantages, such as reliance on molds, lengthy production cycles, low material utilization rate, high material waste, high production cost, limited production volume, poor repeatability, and lack of microstructure control. [29]. These techniques include dry pressing, casting, micromachining, and injection molding [30,31]. Dry pressing and casting have similar limitations, such as the requirement for molds and the inability to produce complex shapes readily [32]. Fractures, porosity, and warpage are a few of the defects that can occur during the dry pressing and casting of ceramics. Nevertheless, these processes are protracted processes that frequently result in a product with an unstable microstructure [30].

Micromachining in ceramics is limited to low-volume production due to the high cost of the required machining tools, the geometric constraints that impede the production of intricate patterns, and the material's fragility [30].

Additive manufacturing (AM) has disrupted the manufacturing space and is being utilized to circumvent the limitations of conventional manufacturing techniques [33–35]. The technique builds monolithic parts layer-by-layer using 3D CAD data, resulting in the fabrication of complex geometries and reducing machining costs [36–38]. The technique provides freedom of design, increased finish quality, and reduced design-to-production lead time [39].

AM techniques have been developed for different materials [40,41], however, the Direct Ink Writing (DIW) technique is the most flexible, which can additively manufacture polymers, metals, ceramics, composites, and biological materials [42–44]. The DIW technique employs viscous pastes termed “inks” to produce monolithic parts [45]. The inks can be loaded with particles of ceramics to produce ceramic green bodies that can be later sintered in a furnace to produce a monolithic ceramic part [46]. Furthermore, pre-ceramic metal powder may also be utilized, which will oxidize in the furnace to produce ceramic parts[47].

The composition of the ink can be customized based on the specific application and desired properties of the printed part [43]. The combination of solid particles, solvents, binders, surfactants, plasticizers, rheology modifiers, and crosslinkers allows for a wide range of ink formulations that can be optimized for different printing methods, materials, and part geometries [45,48–51].

Despite extensive research on DIW of ceramic materials, the additive manufacturing of cupric oxide remains largely unexplored, particularly when derived from metallic copper precursors. Existing DIW studies on ceramics primarily utilize oxide powders, sol–gel routes, or UV-curable suspensions, whereas the transformation of a water-based metallic copper ink into a monolithic CuO ceramic through controlled oxidation and sintering has not been previously reported. In this study, we establish a reproducible process window for printing crack-free CuO structures using an aqueous CMC-based binder formulation with optimized copper loading. The work further demonstrates that the resulting 3D-printed CuO exhibits a combination of high porosity and measurable electrical conductivity, enabling its potential use in sensing and filtration applications. This contribution distinguishes the present study from prior DIW efforts and provides a scalable, low-cost pathway for fabricating functional CuO architectures.

This paper presents the additive manufacturing of copper oxide via the Direct Ink Writing (DIW) technique. A pre-ceramic green body was produced using an aqueous ink loaded with copper particles. The green body was sintered to form a monolithic ceramic part and characterized for its density, structure, and electrical conductivity. The results demonstrate that DIW is a viable technique for the manufacturing of monolithic parts from CuO. Unlike most existing DIW ceramics that utilize oxide powders, sol-gel routes, or UV-curable suspensions, this work establishes the first reported transformation of a water-based metallic copper ink into a monolithic CuO ceramic through a controlled oxidation and sintering process.

2. Materials and methods. - Copper powder, DI water (De-Ionized Water), and CMC (Carboxymethyl Cellulose) binder were the three components used for this research. Copper powder with a particle size of 10µm was purchased and imported from Vanuatu. The DI water was used in this experiment to ensure that no impurity was added to the materials during the manufacturing process, affecting the chemical composition of the slurry. CMC binder, holding CAS number 9000-11-7, was purchased from Purge Chemical Industries, Karachi, Pakistan.

2.1 Preparation of copper-loaded pre-ceramic ink. - The pre-ceramic ink was formulated as a copper particle–laden aqueous binder system. The aqueous binder was first prepared by dissolving 0.20 g of CMC in 10.0 g of deionized water, followed by manual stirring for 3 minutes to ensure complete homogenization. Subsequently, 21.7 g of copper powder was incorporated into the binder solution. The copper powder was added intermittently and stirred continuously to promote uniform wetting and dispersion. Manual stirring throughout this process ensured homogeneous distribution of the metallic particles within the aqueous matrix. The final ink composition on a mass–mass basis consisted of 68.0 wt% copper, 31.3 wt% water, and 0.6 wt% CMC.

Multiple solid loadings were evaluated to identify the optimal formulation for DIW. Copper contents lower than 68 wt% resulted in insufficient structural integrity during drying, leading to cracking of the green bodies. Conversely, higher copper loadings produced excessively dense pastes that consistently clogged the nozzle during extrusion. The polymeric binder concentration also governed drying behaviour: CMC levels above 0.6 wt% increased shrinkage and deformation during solvent removal, whereas lower binder contents led to cracking due to inadequate particle–particle bridging. Based on these observations, the composition of 68.0 wt% Cu and 0.6 wt% CMC in a 31.3 wt% aqueous phase was identified as the optimal mass fraction combination for achieving stable extrusion, shape retention, and crack-free green bodies.

Although the ink was formulated and optimized on a mass–mass basis, its rheological behavior was also considered during process development, as DIW printability is strongly governed by viscosity, shear-thinning characteristics, and yield stress. While full rheological profiling (e.g., viscometry or oscillatory shear measurements) was not performed in this study, the formulation exhibited all qualitative indicators of DIW-compatible flow behavior. Specifically, the ink demonstrated continuous filament formation under extrusion, maintained structural integrity after deposition, and showed no signs of uncontrolled spreading, all of which are consistent with shear-thinning pastes reported in DIW literature. The absence of nozzle clogging or die swell further suggests that the yield stress lies within a suitable range for stable extrusion. The optimized solid and binder mass fractions (68.0 wt% Cu and 0.6 wt% CMC) were therefore selected not only for their influence on drying and green-body integrity, but also for their empirically validated rheological performance during printing.

2.2 Direct Ing Writing. - Parts were manufactured using a modified Creality Ender-3 platform that was adapted for direct ink writing (DIW) through mechanical and control-system modifications. The stock thermoplastic extruder assembly was removed and replaced with a custom-designed DIW print head. The print head consisted of a 50 mL pneumatic dispensing cartridge fitted with a tapered nozzle of 0.4 mm exit diameter, which deposited the copper-loaded pre-ceramic slurry onto a glass build platform. Extrusion was actuated by a regulated pneumatic pressure system (0–1 MPa), supplied by a laboratory compressor and controlled by an electronic solenoid valve interfaced with the printer's control board. Fine adjustment of the extrusion pressure was achieved using an inline pressure regulator to ensure stable and continuous filament formation.

The Ender-3 is originally designed for stepper-driven thermoplastic extrusion and, therefore, its firmware was modified so that the E-axis extrusion commands in the G-code toggled the solenoid valve rather than driving a stepper motor. Geometric parameters, including layer height, nozzle speed, infill pattern, and wall thickness, were defined in the slicing software (Ultimaker Cura), while the extrusion rate was governed exclusively by pneumatic pressure. These modifications enabled reliable deposition of the high-viscosity CuO precursor paste while preserving the positional accuracy inherent to the FFF motion system.

All samples were manufactured under controlled laboratory conditions of 25 ± 1 °C and 50% relative humidity. Fig. 1 illustrates the modified DIW setup along with the part geometry selected for DIW-based CuO ceramic fabrication, and the corresponding DIW process parameters are summarized in Table 1. The printed aerofoil specimen (NACA 2412) had an overall chord length of 100 mm, a maximum thickness of 15.54 mm, and a span of 3 mm (z-axis). The outer shell thickness was set to 0.8 mm, with a rectilinear infill density of 100%. These dimensions were chosen to minimize drying-induced warpage and to promote uniform shrinkage during sintering.

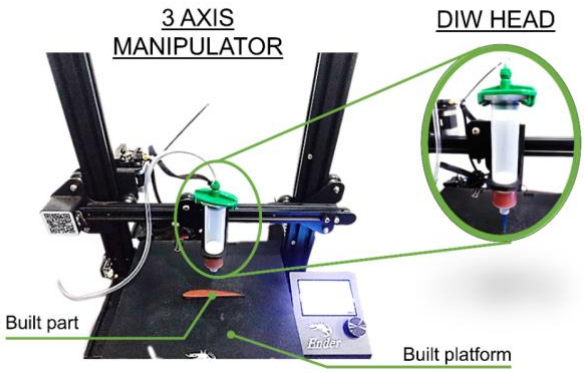

Figure I. The Direct Ink Writing (DIW) setup.

Parameter	Value
Nozzle Diameter	0.4 mm
Layer Height	0.2 mm
Extrusion Width	0.4 mm
Linear Speed	20 $mm.s^{-1}$
Raster Angle	45 degrees
Infill Pattern	Rectilinear
Infill Density	100%
Wall thickness	0.8 mm
Air Pressure	0.2 MPa

Table I. Parameters of the Direct Ink Writing Process.

2.3 Drying, demolding, and sintering. - The printed green bodies were dried at room temperature for 24 h and subsequently sintered in a programmable air furnace concurrently. The temperature schedule consisted of an initial heating step from room temperature to 400 °C at a rate of 5 °C/min, followed by a dwell of 45 min to ensure complete binder burnout. The temperature was then increased from 400 to 900 °C at 5 °C/min, where the samples were held for 180 min to promote oxidation and densification. After sintering, the furnace was allowed to cool naturally to room temperature at an uncontrolled rate. All specimens were sintered in ambient air without additional oxygen flow. The multi-step sintering regime is illustrated in Figure II.

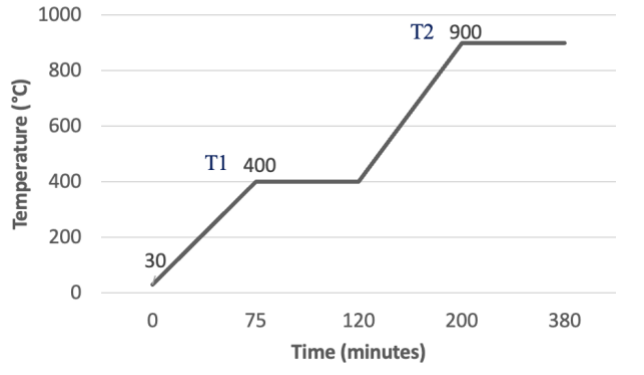

Figure II. The Direct Ink Writing (DIW) setup.

3. Results and discussion. -

3.1 Sintered ceramic body. - The transformation of the DIW sample to the final sintered ceramic body is illustrated in Figure III. The technique can produce monolithic parts using pre-ceramic slurry without cracking and warping. An

isotropic shrinkage of 4.1 ± 0.2 % (n=5) was observed from the CAD model to the sintered body. It can be concluded that the DIW technique is a viable option for the manufacturing of monolithic ceramic parts. Simple and complex part geometries can be designed in a CAD environment and implemented readily for function-specific applications.

Figure III. Transformation from the DIW part to the sintered monolithic ceramic body (Aerofoil Geometry).

3.2 XRD Analysis. - The X-ray diffractogram of the sintered CuO sample is illustrated in Figure IV. The XRD analysis demonstrates that the Cu particles have uniformly oxidized into CuO as the experimental pattern shows an excellent match with the monoclinic CuO reference pattern (Crystallography Open Database) [52]. A quantitative analysis by Rietveld refinement using FullProf software was performed to identify the phase ratio. The results of the refinement indicated that the sample is 99.8 % phase-pure CuO. No significant secondary phases, such as residual Cu or Cu_2O, were detected above the instrument's detection limit.

The degree of crystallinity was determined by integrating the area under the crystalline peaks and the background amorphous hump. Using the peak analyser tool in OriginLab software, the crystallinity degree of the sample was calculated to be 65.78%.

The crystallite size of the XRD patterns was estimated using Scherrer's equation:

$$D = \frac{k\,\lambda}{\beta \cos\theta} \qquad (1)$$

where D is the crystallite size, k is the so-called shape factor (0.9), λ is the wavelength (0.15418 nm, CuKα), β is the Full Width at Half Maximum (FWHM), and θ is the diffraction angle [53]. To ensure an accurate representation, the crystallite size was calculated using the FWHM of the three most intense peaks: $(11\bar{1})$, (111), and (200) located at approximately 35.5°, 38.7°, and 39.8° 2Theta, respectively). The FWHM values were corrected for instrumental broadening using a standard LaB6 reference sample. Exploiting the average of the data derived from these three peaks, an average crystallite size of 71.75 nm was determined, with an estimated standard deviation (error) of 2.1 nm is reported for the measurement. The sample was identified as having a Monoclinic Crystal System with refined lattice parameters.

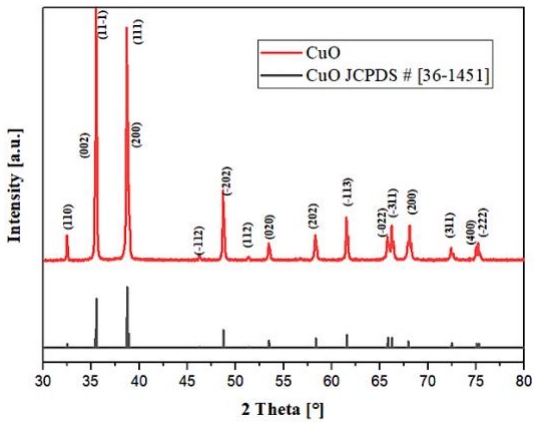

Figure IV. X-ray diffractogram of sintered CuO sample.

The refined lattice parameters of the sintered phase were found to be a = 4.68370 Å, b = 3.42260 Å, c = 5.12880 Å, and β = 99.54°. These values are in excellent agreement with the reported unit-cell dimensions for monoclinic CuO (tenorite), which are typically quoted as a ≈ 4.68 Å, b ≈ 3.42 Å, c ≈ 5.13 Å, and β ≈ 99.5° in standard crystallographic databases and the literature. The close match between the extracted parameters and the reference values indicates that the as-sintered material is phase-pure CuO with negligible lattice distortion. Any minor differences are within expected experimental uncertainty and may arise from instrument calibration, residual micro-strain introduced during the oxidation/sintering cycle, or slight non-stoichiometry. Peak broadening observed in the diffractogram (Scherrer crystallite size ≈ 72 nm) is consistent with the finite crystallite size and could also contribute to small uncertainties in the refined cell metrics.

3.3 Morphology. - The morphology of copper powder and the sintered CuO ceramic was studied under a Scanning Electron Microscope. SEM micrographs of copper powder in Fig. 5 (a and b) depict the powder having an average particle size of 10μm. The SEM micrographs demonstrate the agglomeration of the copper powder. The copper powder was not subjected to ball milling to prevent it from early oxidation.

Figure V (c and d) shows the SEM images of the CuO sintered sample manufactured using additive manufacturing. The micrographs show that powder particles have sintered into a porous structure. This porosity allows for the application of additively manufactured CuO parts in applications such as gas sensing and pollutant filtration [54].

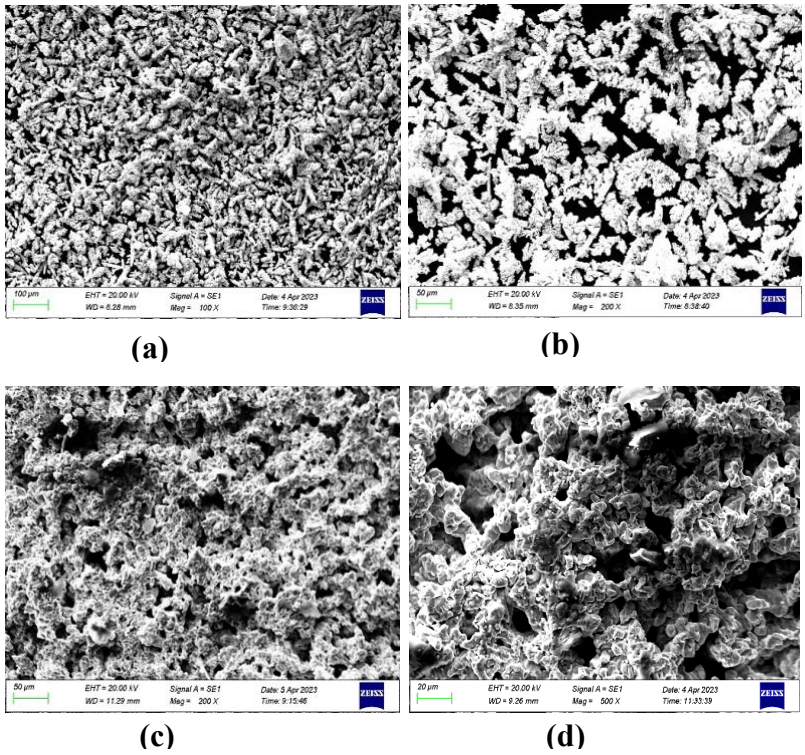

Figure V. (a) SEM image of copper powder at x100 magnification. (b) SEM image of copper powder at x200 magnification. (c) SEM image of sintered CuO ceramic at x200 magnification. (d) SEM image of sintered CuO ceramic at x500 magnification.

3.4 Porosity and Density. - The surface porosity of the sintered sample was estimated through pixel intensity analysis using the ImageJ software. Pixel intensity analysis is illustrated in Figure VI, where the porous regions are mapped with red color. The software estimates a mean surface porosity of 40.4%.

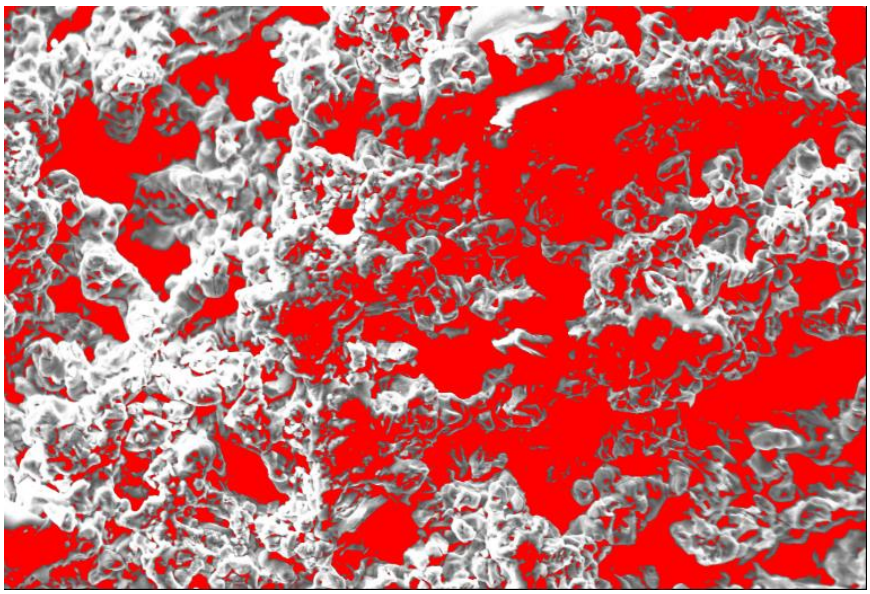

Figure VI. Porosity Analysis of SEM Image of CuO Ceramic Sample using ImageJ Software

The bulk density of the sintered CuO samples was determined using the liquid infiltration method following ASTM C830–00 [55]. Each sample was first weighed in the dry state using an analytical balance to obtain the dry mass (m_{dry}), then immersed in distilled water until complete saturation of open pores was achieved. The samples were gently blotted to remove excess surface liquid and reweighed to obtain the wet mass (m_{wet}).

The bulk volume (V_{bulk}) of each sample was calculated using the relation:

$$V_{bulk} = \frac{m_{dry}}{\rho_{theoratical}} + \frac{m_{wet} - m_{dry}}{\rho_{liquid}} \quad (1)$$

The bulk density of each sample was calculated as:

$$\rho_{bulk} = \frac{m_{dry}}{V_{bulk}} \quad (2)$$

The porosity of each sample was determined by:

$$\%P = 1 - \frac{\rho_{bulk}}{\rho_{theoratical}} \quad (3)$$

The measured dry and wet masses, calculated bulk densities, and porosities for the five samples are summarized in Table 2. The average bulk density was found to be 3.6 ± 0.2 g/cm³, corresponding to a calculated porosity of 43.7 ± 0.9%. The density of the sample can be further increased by secondary infiltration post-sintering for specific applications.

Sample	Dry Mass (g)	Wet Mass (g)	Bulk Density (g/cm³)	Porosity (%)
1	9.45	10.63	3.44	44.6
2	9.75	10.93	3.57	44.3
3	9.95	11.14	3.61	43.7
4	10.20	11.40	3.65	42.9
5	10.45	11.68	3.69	42.3

Table II. Results of bulk density measurements.

The close agreement between the bulk (43.7%) and surface (40.4%) porosity values confirms that the CuO ceramic exhibits a homogeneously distributed porous microstructure. The slight variance, where the bulk value is marginally higher, is primarily attributed to the inclusion of closed porosity in the 3D density calculation, which is inherently

excluded from the 2D surface projection, further supporting the conclusion that the additive manufacturing approach successfully produced a high-porosity ceramic structure suitable for the intended applications.

3.5 Resistivity Analysis. - The resistivity was determined using the four-probe resistivity technique [56]. The voltage was measured at the two inner probes, while the current was injected using the two outer probes. The schematic of the four-probe resistivity technique is illustrated in Figure VII.

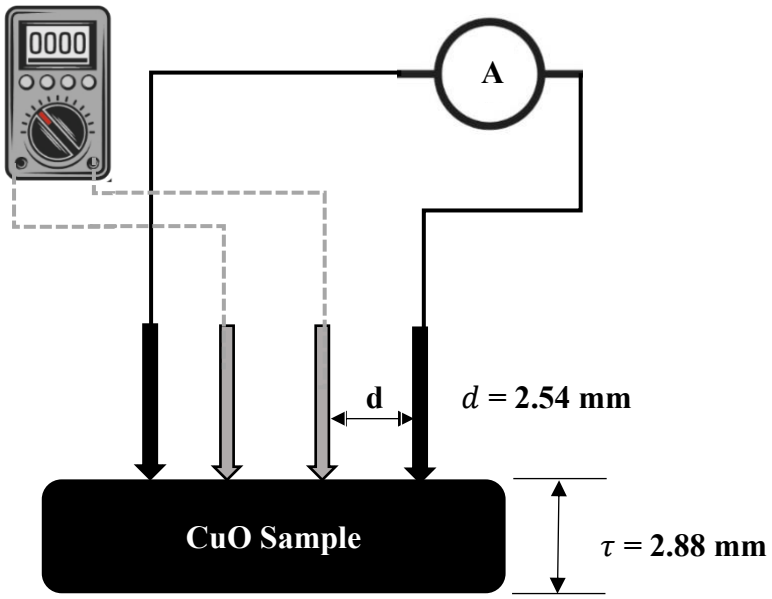

Figure VII. The schematic of the four-probe resistivity technique.

The printed and sintered CuO aerofoil samples had an average thickness of 2.88 mm, while the probe spacing (d) of the four-point probe head was fixed at 2.54 mm. The measurements were performed directly on the as-sintered surface without additional polishing or metallization, as the intrinsic conductivity of the CuO matrix was sufficient for stable contact formation. All measurements were conducted at a controlled room temperature of 25 ± 1°C and 50% relative humidity. To ensure the validity of the measurement, the current *I* was swept across a range of 1 mA to 10 mA, and the resulting *I-V* curve was confirmed to be linear ($R^2 > 0.999$), indicating Ohmic contact behavior within the measurement range and validating the use of the following resistivity formula for bulk material:

The computations were conducted using the resistivity formula for the bulk material [54].

$$\rho = \frac{V}{I}\, x\, \frac{\pi\, \tau}{\ln\left(\frac{\sinh\,(\tau/d)}{\sinh\,(\tau/2d)}\right)} \qquad (4)$$

where V is the recorded voltage, I is the injected current, τ is the thickness of the sample, and d is the probe spacing. The resistivity of the CuO sample was computed to be 10.5 ± 0.3 $\Omega\, m$ (n=5) which corresponds to a conductivity of (9.5 ± 0.3) $x10^{-2}$ S/m.

The electrical conductivity indicates the potential for the additively manufactured CuO parts to function as active components, such as electrodes or catalytic membranes. This is enabled by the synergy between this foundational conductivity and the high surface area derived from the 43.7 % theoretical porosity. Therefore, while the bulk electrical measurement establishes the viability for charge conduction, the true potential for specific applications, including electrochemical sensing, supercapacitors, and heterogeneous catalysis, must be confirmed through subsequent device-level proof-of-concept (PoC) studies that evaluate charge transfer kinetics and functional performance.

3.6 Efficacy of the DIW technique. - The results demonstrate that the DIW technique is a viable alternative to produce monolithic ceramic parts from CuO, circumventing the limitations of conventional ceramic manufacturing techniques. Complex geometries could be designed in a CAD environment and manufactured readily. The SEM, porosity, and XRD analyses show that the resulting part shall be porous and may be employed in various applications such as filtering of microbial and chemical pollutants. The electrical conductivity will enable the utilization of the sintered part in biological sensing and gas sensing applications. The developed technique can be explored for the manufacturing of other functional metal oxides, such as Al2O3 and TiO2.

The physical and electrical properties achieved via this novel Direct Ink Writing (DIW) route demonstrate a successful balance between a desirable architecture and inherent material characteristics when compared to traditional CuO ceramics and functional films.

The measured bulk density of 3.60 ± 0.20 g/cm³ is significantly lower than the theoretical density of fully dense CuO (often cited near 6.31 g/cm³ [52]), which is a direct consequence of the resulting high porosity of 40.4%. This structured, high-porosity is a key feature of the DIW process, ensuring the high surface area required for functional applications such as gas sensors and catalytic applications, where morphology and enhanced surface reaction sites are critical for performance [22].

Furthermore, the measured bulk resistivity of 10.5 ± 0.3 Ω m is characteristic of the material's semiconducting behavior. CuO is widely studied as a p-type semiconductor [23], and this resistivity confirms that the 3D-printed, porous ceramic possesses the required electrical properties to function as an active layer in conductometric devices, distinguishing it from fully insulating ceramic structures [23].

Despite the functional advantages of high porosity, this architecture presents inherent trade-offs, which must be acknowledged. This high porosity inherently limits mechanical strength and structural rigidity. The interconnected pore network facilitates charge transport pathways and enhances active surface exposure, but it also reduces the load-bearing solid fraction, making the parts more susceptible to brittle failure under mechanical stress.

Similarly, the measured bulk resistivity of 10.5 ± 0.3 Ω m is characteristic of the material's p-type semiconducting behaviour [23], but is significantly higher than that of dense sintered CuO. This elevated resistivity reflects both the porous morphology and the reduced percolation pathways for charge transport. The presence of air-filled voids, oxide necks between particles, and incomplete densification restricts electron mobility, further illustrating an intrinsic trade-off between porosity-driven functional advantages and the deterioration of both electrical and mechanical properties. Future studies should therefore focus on tuning the sintering schedule, solid loading, or post-processing treatments (e.g., partial densification, infiltration) to balance porosity with improved conductivity and structural robustness depending on the intended application.

4. Conclusion. - This study demonstrated the successful fabrication of porous CuO ceramics using a direct ink writing (DIW) route starting from a copper particle–laden aqueous binder system. The optimized ink formulation (68.0 wt% Cu, 31.3 wt% water, and 0.6 wt% CMC) enabled stable extrusion and the formation of crack-free green bodies. Following oxidation and sintering, the printed structures exhibited a bulk density of 3.60 ± 0.20 g/cm³, corresponding to a theoretical porosity of 43.7 ± 0.9 %. SEM analysis confirmed a porous interconnected microstructure and the formation of monoclinic CuO as the dominant crystalline phase.

Electrical characterization using a four-point probe configuration yielded a bulk resistivity of 10.5 ± 0.3 Ω m and a corresponding conductivity of $(9.5 \pm 0.3) \times 10^{-2}$ S/m at 25 ± 1 °C. These values reflect the influence of the high porosity and incomplete densification on charge-transport behavior. The combined microstructural and electrical results indicate that the additively manufactured CuO components possess the foundational properties required for functional applications where surface area, diffusion, and moderate conductivity are desirable.

While the present work establishes the feasibility of DIW-based CuO fabrication, the potential applicability of these structures in gas sensing, filtration, catalysis, or electrochemical systems remains conditional and will require dedicated device-level testing to evaluate performance, stability, and charge-transfer characteristics. Future studies may focus on controlling densification, tailoring porosity, or incorporating post-processing treatments to further optimize the balance between electrical, structural, and functional requirements.

Declaration Conflict of Interest. - The authors of this research announce that they have no known contending monetary interests or individual connections that may have impacted the work detailed in this paper.

Data and Code Availability. - Data and code shall be made available upon request to the corresponding author.

References

[1] W.R. Matizamhuka, Advanced ceramics — The new frontier in modern-day technology: Part I, J South Afr Inst Min Metall 118 (2018) 757–764. https://doi.org/10.17159/2411-9717/2018/V118N7A9.

[2] T. Ayode Otitoju, P. Ugochukwu Okoye, G. Chen, Y. Li, M. Onyeka Okoye, S. Li, Advanced ceramic components: Materials, fabrication, and applications, Journal of Industrial and Engineering Chemistry 85 (2020) 34–65. https://doi.org/10.1016/J.JIEC.2020.02.002.

[3] C.Barry. Carter, M.Grant. Norton, Ceramic materials: science and engineering, (2013). https://books.google.com/books/about/Ceramic_Materials.html?id=WRg_AAAAQBAJ (accessed March 26, 2023).

[4] R. Danzer, On the relationship between ceramic strength and the requirements for mechanical design, J Eur Ceram Soc 34 (2014) 3435–3460. https://doi.org/10.1016/J.JEURCERAMSOC.2014.04.026.

[5] F. Klocke, Modern approaches for the production of ceramic components, J Eur Ceram Soc 17 (1997) 457–465. https://doi.org/10.1016/S0955-2219(96)00163-X.

[6] H. Budharaju, S. Suresh, M.P. Sekar, B. De Vega, S. Sethuraman, D. Sundaramurthi, D.M. Kalaskar, Ceramic materials for 3D printing of biomimetic bone scaffolds – Current state-of-the-art & future perspectives, Mater Des 231 (2023) 112064. https://doi.org/10.1016/J.MATDES.2023.112064.

[7] M. Laborie, A. Naveau, A. Menard, CAD-CAM resin-ceramic material wear: A systematic review, J Prosthet Dent (2022). https://doi.org/10.1016/J.PROSDENT.2022.01.027.

[8] Susilawati, T.I. Nasution, M. Hasanah, Y.A. Sihombing, Fabrication of Ceramic Composites Based on CuO-ZnO, (2018). https://dupakdosen.usu.ac.id/handle/123456789/69927 (accessed April 1, 2023).

[9] D. Renuga, J. Jeyasundari, S. Athithan, Y. Brightson, A. Jacob, Synthesis and characterization of copper oxide nanoparticles using Brassica oleracea var. italic extract for its antifungal application, Mater. Res. Express 7 (2020) 45007. https://doi.org/10.1088/2053-1591/ab7b94.

[10] S. Steinhauer, E. Brunet, T. Maier, G.C. Mutinati, A. Köck, O. Freudenberg, C. Gspan, W. Grogger, A. Neuhold, R. Resel, Gas sensing properties of novel CuO nanowire devices, Sens Actuators B Chem 187 (2013) 50–57. https://doi.org/10.1016/J.SNB.2012.09.034.

[11] D.G. Desai, G.R. Navale, D.J. Late, M.S. Dharne, P.S. Walke, Size does matter: antibacterial activities and cytotoxic evaluation of polymorphic CuO nanostructures, J Mater Sci 58 (2023) 2782–2800. https://doi.org/10.1007/S10853-023-08157-4/METRICS.

[12] A.P. Cabello, M.A. Ulla, J.M. Zamaro, In situ growth of nanostructured copper and zinc mixed oxides on brass supports as efficient microreactors for the catalytic CO oxidation, Journal of Materials Science 2022 57:27 57 (2022) 12797–12809. https://doi.org/10.1007/S10853-022-07391-6.

[13] B.K. Singh, State-of-Art on Self-Lubricating Ceramics and Application of Cu/CuO as Solid Lubricant Material, Https://Doi.Org/10.1080/0371750X.2022.2149625 (2023). https://doi.org/10.1080/0371750X.2022.2149625.

[14] L.E. Román, C. Villalva, C. Uribe, F. Paraguay-Delgado, J. Sousa, J. Vigo, C.M. Vera, M.M. Gómez, J.L. Solís, Textiles Functionalized with Copper Oxides: A Sustainable Option for Prevention of COVID-19, Polymers 2022, Vol. 14, Page 3066 14 (2022) 3066. https://doi.org/10.3390/POLYM14153066.

[15] A.M. Anand, A. Raj, R. Adithya Nath, J.A. Salam, R. Jayakrishnan, Self-powered UV photodetector based on self-assembled CuO and spin-coated ZnO heterostructure, J Mater Sci 58 (2023) 11000–11015. https://doi.org/10.1007/S10853-023-08726-7/METRICS.

[16] R. Ahmad, M. Vaseem, N. Tripathy, Y.B. Hahn, Wide linear-range detecting nonenzymatic glucose biosensor based on CuO nanoparticles inkjet-printed on electrodes, Anal Chem 85 (2013) 10448–10454. https://doi.org/10.1021/AC402925R.

[17] K. Abdelkarem, R. Saad, A.M. Ahmed, M.I. Fathy, M. Shaban, H. Hamdy, Efficient room temperature carbon dioxide gas sensor based on barium doped CuO thin films, J Mater Sci 58 (2023) 11568–11584. https://doi.org/10.1007/S10853-023-08687-X/TABLES/3.

[18] D.Y. Tiba, L.L. Name, R. Landers, T.C. Canevari, Copper oxide nanostructures with nanoneedles shape obtained by direct reaction with nitrogen-doped carbon quantum dots: development of an electrochemical sensor to glyphosate, J Mater Sci 58 (2023) 12569–12583. https://doi.org/10.1007/S10853-023-08827-3/METRICS.

[19] U.A.A. Yasin, M.M. Ahmed, J. Zhang, Z. Jia, T. Guo, R. Zhao, J. Shi, J. Du, Engineering the band structure of CuO via decoration with AgBr to enhance its photocatalytic degradation performance, J Mater Sci 58 (2023) 7333–7346. https://doi.org/10.1007/S10853-023-08487-3/METRICS.

[20] N. Bin Tanvir, C. Wilbertz, S. Steinhauer, A. Köck, G. Urban, O. Yurchenko, Work Function Based CO2 Gas Sensing Using Metal Oxide Nanoparticles at Room Temperature, Mater Today Proc 2 (2015) 4190–4195. https://doi.org/10.1016/J.MATPR.2015.09.002.
[21] O. Baranov, K. Bazaka, T. Belmonte, C. Riccardi, H.E. Roman, M. Mohandas, S. Xu, U. Cvelbar, I. Levchenko, Recent innovations in the technology and applications of low-dimensional CuO nanostructures for sensing, energy and catalysis, Nanoscale Horiz (2023). https://doi.org/10.1039/D2NH00546H.
[22] O. Lupan, V. Postica, N. Ababii, M. Hoppe, V. Cretu, I. Tiginyanu, V. Sontea, T. Pauporté, B. Viana, R. Adelung, Influence of CuO nanostructures morphology on hydrogen gas sensing performances, Microelectron Eng 164 (2016) 63–70. https://doi.org/10.1016/J.MEE.2016.07.008.
[23] F. Shao, F. Hernández-Ramírez, J.D. Prades, C. Fàbrega, T. Andreu, J.R. Morante, Copper (II) oxide nanowires for p-type conductometric NH 3 sensing, Appl Surf Sci 311 (2014) 177–181. https://doi.org/10.1016/J.APSUSC.2014.05.038.
[24] S. Wang, S. Gao, J. Tian, Q. Wang, T. Wang, X. Hao, F. Cui, A stable and easily prepared copper oxide catalyst for degradation of organic pollutants by peroxymonosulfate activation, J Hazard Mater 387 (2020) 121995. https://doi.org/10.1016/J.JHAZMAT.2019.121995.
[25] T.H. Tran, V.T. Nguyen, Review Article Copper Oxide Nanomaterials Prepared by Solution Methods, Some Properties, and Potential Applications: A Brief Review, (2014). https://doi.org/10.1155/2014/856592.
[26] J.O. Ighalo, P.A. Sagboye, G. Umenweke, O.J. Ajala, F.O. Omoarukhe, C.A. Adeyanju, S. Ogunniyi, A.G. Adeniyi, CuO nanoparticles (CuO NPs) for water treatment: A review of recent advances, Environ Nanotechnol Monit Manag 15 (2021). https://doi.org/10.1016/J.ENMM.2021.100443.
[27] S. Saif, S.F. Adil, M. Khan, M.R. Hatshan, M. Khan, F. Bashir, Adsorption Studies of Arsenic(V) by CuO Nanoparticles Synthesized by Phyllanthus emblica Leaf-Extract-Fueled Solution Combustion Synthesis, Sustainability 2021, Vol. 13, Page 2017 13 (2021) 2017. https://doi.org/10.3390/SU13042017.
[28] L. Mohammadi, E. Bazrafshan, M. Noroozifar, A. Ansari-Moghaddam, F. Barahuie, D. Balarak, Adsorptive Removal of Benzene and Toluene from Aqueous Environments by Cupric Oxide Nanoparticles: Kinetics and Isotherm Studies, J Chem 2017 (2017). https://doi.org/10.1155/2017/2069519.
[29] Z. Liu, C. Ma, Z. Chang, P. Yan, F. Li, Advances in crack formation mechanism and inhibition strategy for ceramic additive manufacturing, J Eur Ceram Soc 43 (2023) 5078–5098. https://doi.org/10.1016/J.JEURCERAMSOC.2023.05.008.
[30] S.S. Hossain, K. Lu, Recent progress of alumina ceramics by direct ink writing: Ink design, printing and post-processing, Ceram Int 49 (2023) 10199–10212. https://doi.org/10.1016/J.CERAMINT.2023.01.143.
[31] J. xin Wen, T. bin Zhu, Z. peng Xie, W. bin Cao, W. Liu, A strategy to obtain a high-density and high-strength zirconia ceramic via ceramic injection molding by the modification of oleic acid, International Journal of Minerals, Metallurgy and Materials 24 (2017) 718–725. https://doi.org/10.1007/S12613-017-1455-9/METRICS.
[32] S.M. Olhero, P.M.C. Torres, J. Mesquita-Guimarães, J. Baltazar, J. Pinho-da-Cruz, S. Gouveia, Conventional versus additive manufacturing in the structural performance of dense alumina-zirconia ceramics: 20 years of research, challenges and future perspectives, J Manuf Process 77 (2022) 838–879. https://doi.org/10.1016/J.JMAPRO.2022.02.041.
[33] A. Vevers, A. Kromanis, E. Gerins, J. Ozolins, Additive Manufacturing and Casting Technology Comparison: Mechanical Properties, Productivity and Cost Benchmark, Latvian Journal of Physics and Technical Sciences 55 (2018) 56–63. https://doi.org/10.2478/LPTS-2018-0013.
[34] Y. Lin, D. Wang, C. Yang, W. Zhang, Z. Wang, An Al-Al interpenetrating-phase composite by 3D printing and hot extrusion, International Journal of Minerals, Metallurgy and Materials 30 (2023) 678–688. https://doi.org/10.1007/S12613-022-2543-Z/METRICS.
[35] Y. tao Gao, T. hua Wu, Y. Zhou, Application and prospective of 3D printing in rock mechanics: A review, International Journal of Minerals, Metallurgy and Materials 28 (2021) 1–17. https://doi.org/10.1007/S12613-020-2119-8/METRICS.
[36] A. Zocca, P. Colombo, C.M. Gomes, J. Günster, Additive Manufacturing of Ceramics: Issues, Potentialities, and Opportunities, Journal of the American Ceramic Society 98 (2015) 1983–2001. https://doi.org/10.1111/JACE.13700.
[37] R. Galante, C.G. Figueiredo-Pina, A.P. Serro, Additive manufacturing of ceramics for dental applications: A review, Dental Materials 35 (2019) 825–846. https://doi.org/10.1016/J.DENTAL.2019.02.026.

[38] B. Diepold, N. Vorlaufer, S. Neumeier, T. Gartner, M. Göken, Optimization of the heat treatment of additively manufactured Ni-base superalloy IN718, International Journal of Minerals, Metallurgy and Materials 27 (2020) 640–648. https://doi.org/10.1007/S12613-020-1991-6/METRICS.
[39] S. Ford, M. Despeisse, Additive manufacturing and sustainability: an exploratory study of the advantages and challenges, J Clean Prod 137 (2016) 1573–1587. https://doi.org/10.1016/J.JCLEPRO.2016.04.150.
[40] M. Srivastava, S. Rathee, V. Patel, A. Kumar, P.G. Koppad, A review of various materials for additive manufacturing: Recent trends and processing issues, (2022). https://doi.org/10.1016/j.jmrt.2022.10.015.
[41] H. Liu, J. Wu, S. Wang, J. Duan, H. Shao, Effect of Sr2+ on 3D gel-printed Sr3−xMgx(PO4)2 composite scaffolds for bone tissue engineering, International Journal of Minerals, Metallurgy and Materials 30 (2023) 2236–2244. https://doi.org/10.1007/S12613-023-2638-1/METRICS.
[42] M.A.S.R. Saadi, A. Maguire, N.T. Pottackal, M.S.H. Thakur, M.M. Ikram, A.J. Hart, P.M. Ajayan, M.M. Rahman, Direct Ink Writing: A 3D Printing Technology for Diverse Materials, Advanced Materials 34 (2022). https://doi.org/10.1002/ADMA.202108855.
[43] S.B. Balani, S.H. Ghaffar, M. Chougan, E. Pei, E. Şahin, Processes and materials used for direct writing technologies: A review, Results in Engineering 11 (2021) 100257. https://doi.org/10.1016/J.RINENG.2021.100257.
[44] S.A. Khan, I. Lazoglu, Development of additively manufacturable and electrically conductive graphite–polymer composites, Progress in Additive Manufacturing 5 (2020) 153–162. https://doi.org/10.1007/s40964-019-00102-9.
[45] L. del-Mazo-Barbara, M.P. Ginebra, Rheological characterisation of ceramic inks for 3D direct ink writing: A review, J Eur Ceram Soc 41 (2021) 18–33. https://doi.org/10.1016/J.JEURCERAMSOC.2021.08.031.
[46] F. Abdeljawad, D.S. Bolintineanu, A. Cook, H. Brown-Shaklee, C. DiAntonio, D. Kammler, A. Roach, Sintering processes in direct ink write additive manufacturing: A mesoscopic modeling approach, Acta Mater 169 (2019) 60–75. https://doi.org/10.1016/J.ACTAMAT.2019.01.011.
[47] S.A. Legett, X. Torres, A.M. Schmalzer, A. Pacheco, J.R. Stockdale, S. Talley, T. Robison, A. Labouriau, Balancing Functionality and Printability: High-Loading Polymer Resins for Direct Ink Writing, Polymers 2022, Vol. 14, Page 4661 14 (2022) 4661. https://doi.org/10.3390/POLYM14214661.
[48] D. Graf, J. Jung, T. Hanemann, Formulation of a Ceramic Ink for 3D Inkjet Printing, Micromachines (Basel) 12 (2021). https://doi.org/10.3390/MI12091136.
[49] Y. De Hazan, J. Heinecke, A. Weber, T. Graule, High solids loading ceramic colloidal dispersions in UV curable media via comb-polyelectrolyte surfactants, J Colloid Interface Sci 337 (2009) 66–74. https://doi.org/10.1016/J.JCIS.2009.05.012.
[50] Z. Xing, W. Liu, Y. Chen, W. Li, Effect of plasticizer on the fabrication and properties of alumina ceramic by stereolithography-based additive manufacturing, Ceram Int 44 (2018) 19939–19944. https://doi.org/10.1016/J.CERAMINT.2018.07.259.
[51] T. Chen, A. Sun, C. Chu, H. Wu, J. Wang, J. Wang, Z. Li, J. Guo, G. Xu, Rheological behavior of titania ink and mechanical properties of titania ceramic structures by 3D direct ink writing using high solid loading titania ceramic ink, J Alloys Compd 783 (2019) 321–328. https://doi.org/10.1016/J.JALLCOM.2018.12.334.
[52] S. Gražulis, A. Daškevič, A. Merkys, D. Chateigner, L. Lutterotti, M. Quirós, N.R. Serebryanaya, P. Moeck, R.T. Downs, A. Le Bail, Crystallography Open Database (COD): An open-access collection of crystal structures and platform for world-wide collaboration, Nucleic Acids Res 40 (2012). https://doi.org/10.1093/NAR/GKR900.
[53] J.I. Langford, X-ray diffraction procedures for polycrystalline and amorphous materials by H. P. Klug and L. E. Alexander, J Appl Crystallogr 8 (1975) 573–574. https://doi.org/10.1107/S0021889875011399.
[54] D. Jung, S. Hwang, H.J. Kim, J.H. Han, H.N. Lee, Characterization of Porous CuO Films for H2S Gas Sensors, Materials 15 (2022) 7270. https://doi.org/10.3390/MA15207270/S1.
[55] A. Shahzad, S.A. Khan, A. Paksoy, Ö. Balcı-Çağıran, I. Lazoglu, Negative additive manufacturing of Al2O3-Al cermet material by fused deposition and Direct Ink Writing, Mater Today Commun 33 (2022). https://doi.org/10.1016/J.MTCOMM.2022.104739.
[56] D. Schroder, Semiconductor material and device characterization, IEEE Press; Wiley, Piscataway NJ; Hoboken N.J., 2006.

Author contribution:

1. Conception and design of the study

2. Data acquisition

3. Data analysis

4. Discussion of the results

5. Writing of the manuscript

6. Approval of the last version of the manuscript

MA has contributed to: 1, 2, 3, 4, 5 and 6.

SAK has contributed to: 1, 2, 3, 4, 5 and 6.

AS has contributed to: 1, 2, 3, 4, 5 and 6.

AN has contributed to: 1, 2, 3, 4, 5 and 6.

AH has contributed to: 1, 2, 3, 4, 5 and 6.

Acceptance Note: This article was approved by the journal editors Dr. Rafael Sotelo and Mag. Ing. Fernando A. Hernández Gobertti.